Catalysis Science & Technology

ROYAL SOCIETY OF CHEMISTRY

PAPER

Cite this: *Catal. Sci. Technol.*, 2021, 11, 6866

Vapor-phase conversion of aqueous 3-hydroxybutyric acid and crotonic acid to propylene over solid acid catalysts†

Shijie Leow, ‡§[abc] Andrew J. Koehler, ‡[abd] Lauren E. Cronmiller, [ab] Xiangchen Huo,[ad] Gabriella D. Lahti, [d] Yalin Li, [abc] Glenn R. Hafenstine, [d] Derek R. Vardon *[d] and Timothy J. Strathmann *[ab]

Diverse sources of wastewater organic carbon can be microbially funneled into biopolymers like polyhydroxybutyrate (PHB) that can be further valorized by conversion to hydrocarbon fuels and industrial chemicals. We report the vapor-phase dehydration and decarboxylation of PHB-derived monomer acids, 3-hydroxybutyric acid (3HB) and crotonic acid (CA), in water to propylene over solid acid catalysts using a packed-bed continuous-flow reactor. Propylene yields increase with increased Brønsted acidity of catalysts, with amorphous silica–alumina and niobium phosphate yielding 52 and 60 %C (percent feedstock carbon, max 75 %C) of feedstock 3HB and CA, respectively; additional products include CO_2 and retro-aldol products (acetaldehyde and acetic acid). Deactivation studies indicate progressive and permanent steam deactivation of amorphous silica–alumina, while re-calcination partially recovers niobium phosphate activity. Experiments demonstrating sustained reactor operation over niobium phosphate provide a promising technology pathway for increasing valorization of organic-rich wastewater.

Received 29th June 2021,
Accepted 29th August 2021

DOI: 10.1039/d1cy01152a

rsc.li/catalysis

Introduction

Growing urbanization has increased societal energy demands, greenhouse gas emissions, and wastewater generation. Simultaneously addressing these changes contributes to a growing impetus for wastewater treatment plants (WWTPs) to transition into renewable resource production facilities capable of valorizing organic wastes into petrochemical replacements while meeting treated water quality requirements.[1,2] Recent developments posit that organic carbon and nutrients in domestic and industrial wastewaters can be funneled through biological accumulation of storage products (*e.g.*, bacterial biopolymers or microalgal fatty acids),[3,4] which can subsequently be processed through nascent biorefinery technologies into more energy-dense and valuable commercial products (*e.g.*, renewable liquid fuel blendstocks or commodity chemicals).[5,6] This pathway offers the potential for a greater variety of alternative products from wastewater carbon with higher values than conventional anaerobic digestion processes aimed at producing methane-containing biogas.[3,4]

One promising strategy involves retrofitting conventional WWTP processes to yield biomass enriched in the biopolymer polyhydroxybutyrate (PHB; a polyester of 3-hydroxybutyric acid or 3HB; Fig. 1) for use in biorenewable materials (*e.g.*, bioplastics).[7] Reports demonstrate treatment of wastewater to regulatory standards at the pilot-scale

[a] *Department of Civil and Environmental Engineering, Colorado School of Mines, 1500 Illinois St., Golden, CO 80401, USA. E-mail: strthmnn@mines.edu*
[b] *Engineering Research Center for Re-inventing the Nation's Urban Water Infrastructure (ReNUWIt), Colorado School of Mines, Golden, CO 80401, USA*
[c] *Department of Civil and Environmental Engineering, University of Illinois at Urbana-Champaign, Newmark Civil Engineering Laboratory, 205 N. Matthews Ave., Urbana, IL 61801, USA*
[d] *National Renewable Energy Laboratory, 15013 Denver West Parkway, Golden, CO 80401, USA. E-mail: Derek.Vardon@nrel.gov*

† Electronic supplementary information (ESI) available. See DOI: 10.1039/d1cy01152a

‡ S. L. and A. K. should be considered joint first author.

§ Current affiliation: Nanyang Technological University, Nanyang Environment & Water Research Institute, 1 Cleantech Loop, CleanTech One, #06-08, 637 141, Singapore.

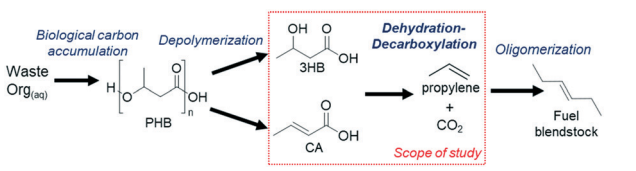

Fig. 1 Proposed integrated processing schematic for valorization of wastewater organic carbon *via* biological accumulation of PHB and conversion to propylene and renewable hydrocarbon fuel blendstocks. The scope of this study focuses on vapor-phase catalytic conversion of 3HB and CA acid monomers to propylene *via* dehydration and decarboxylation reactions (dashed red box).

concurrent with selection of PHB-accumulating mixed cultures, with PHB accumulation of up to 50–90% cell dry weight.[8–10] These reports show clear potential for integration of PHB production with waste treatment operations.[11–13] However, widespread commercial application of PHB as a bioplastic still requires significant scientific advances addressing the use of costly organic solvents for product extraction and recovery,[14,15] achieving suitable material property standards for biopolymer applications, and integrated process demonstrations of waste feedstocks (*e.g.*, wastewater digested sludge, food waste, *etc.*) to fungible PHB plastics at larger scales.[14–16]

As an alternative to direct use, pathways converting PHB to platform chemicals have emerged with particular emphasis on the production of propylene, valued as a commodity feedstock for chemicals or as a precursor to liquid renewable hydrocarbon fuel blendstocks.[17] Direct conversion of PHB to propylene has been shown through batch reactions leveraging techniques such thermolysis,[18] catalytic pyrolysis,[19] and catalytic reforming.[20] While most reports of biological PHB production have focused on the use of purified sugars as feedstocks, costs are lower when sourcing organic carbon from wastewater streams.[21] In either case, developing pathways that limit costly dewatering and drying steps prior to any downstream separation and conversion reactions are ideal for energy reduction.[22,23]

As an alternative to dry solvent extraction techniques, PHB can be separated from wet cell biomass using mild aqueous-phase techniques.[24,25] Subsequent depolymerization reactions can then produce a concentrated aqueous mixture of acid monomers, 3-hydroxybutyric acid (3HB) and crotonic acid (CA).[12,26] Batch reactions involving direct hydrothermal conversion of PHB and its monomer acids to propylene have been recently explored,[25,27,28] but to date there have been no reports on continuous aqueous-phase conversion of PHB or its monomer acids to propylene. Building upon recent reports of vapor-phase catalytic conversion of γ-valerolactone to butenes,[17,29] we hypothesized that dehydration and decarboxylation reactions of 3HB and CA that yield propylene (Fig. 1) will also be promoted by solid acid catalysts, including commercially available amorphous silica–alumina and emerging niobium-based acid catalysts. Vapor-phase catalytic reactions enable low pressure chemistry (<4 atm) with lower reactor capital requirements, which can be compatible with upstream dewatering technologies that further concentrate the aqueous feed stream before reaching dryness. This process is advantageous for the conversion of 3HB, providing improved control over yields and product selectivity compared to catalytic pyrolysis and hydrothermal reforming which yield under 50 mol% propylene conversion from PHB.[19,27] Additionally, the volatility of propylene enables self-separation from the aqueous process stream, lowering expected costs for product separation and enabling purification as an industrial feedstock chemical or oligomerization to produce liquid renewable hydrocarbon fuel blendstocks.

A growing body of literature has reported on the application of solid acid catalysts for conversion of biomass-derived chemicals, including triglycerides,[30] sugars,[31] and lignocellulosics.[32] Use of solid acid catalysts can reduce cost, corrosion, and waste associated with homogenous catalysts.[33] Amorphous silica–alumina catalysts have been found to be desirable for biomass conversions due to their low cost, commercial availability, and variable Brønsted and Lewis acidities.[34–36] More recently, niobium-based acid catalysts have been explored as alternatives for dehydration, hydrolysis, and esterification reactions of biomass.[37] Bulk niobium-based catalysts are of particular interest due to their strong water-tolerant acidity,[38,39] with niobium frequently added to other catalysts to increase hydrothermal stability. Recent reports suggest that bulk niobium oxides are not hydrothermally stable (evidenced by decreased surface area),[40,41] but some studies suggest stable catalytic performance when exposed to heated water vapor.[42] Niobium phosphate is particularly promising for these applications due to stronger acidity and greater thermal stability than niobic acid.[43] To our knowledge, there have been no reports of PHB-derived monomer acid reactions with either silica–alumina or niobium-based catalysts.

This study reports the vapor-phase catalytic reactions of PHB-derived monomer acids, 3HB and CA, focusing on optimizing propylene yields and selectivity, as well as catalyst stability. Reactions were studied using a continuous flow packed-bed reactor incorporating commercially available solid acid catalysts (alumina, amorphous silica–alumina, and niobium-based materials) to evaluate the effect of varying Brønsted–Lewis acidities on acid conversion and product selectivity. Experiments were also conducted to evaluate catalyst stability and deactivation, including experiments exposing catalysts to superheated steam for an extended period prior to introducing 3HB feeds and an extended CA partial conversion experiment to monitor catalyst deactivation and re-activation *via* calcination. Activity measurements were coupled with materials characterization to evaluate catalyst properties and identify potential modes of deactivation and regeneration potential. Results from this work provide mechanistic insights into the conversion reactions and important catalyst properties as well as factors limiting catalyst stability that are critical to further development of a practical catalytic conversion technology for PHB-derived monomer acids. Ultimately, these processes can be incorporated within a larger PHB-to-fuel pathway, providing a path forward towards the realization of renewable fuel production from wastewater organic carbon.

Materials and methods

Reagents and catalysts

Amorphous silica–alumina catalysts (DAVICAT® SIAL 3113 and SIAL 3125) were acquired from Grace-Davison. The catalysts contained 13 and 25 wt% alumina respectively, as denoted by the manufacturer. A Na^+-exchanged SIAL 3113

was prepared to selectively poison Brønsted acid sites following a procedure described by Foo *et al.*[44] γ-Al_2O_3 was obtained from Strem Chemicals (13-2525). Niobic acid (NbO) and niobium phosphate (NbP) were provided by Companhia Brasileira de Metalurgia e Mineração (CBMM). Prior to use, all catalysts were calcined in air for 3 hours with a 200 °C h^{-1} heat-up rate with no further modifications. SIAL 3113, SIAL 3125, γ-Al_2O_3, and Na^+-exchanged SIAL 3113 were calcined at 450 °C.[45] NbO and NbP were calcined at 400 °C.[46]

Flow reactor experiments and product analysis

Continuous flow experiments (6 h time-on-stream) for catalytic conversion of 3HB and CA were carried out in a packed-bed down-flow continuous reactor (photograph and schematic shown in Fig. S1 in the ESI†). Aqueous solutions of monomer acid in water (20 g L^{-1}) were delivered (0.3 mL min^{-1} typically, or adjusted as necessary depending on the tested catalyst to maintain a WHSV of 0.1 h^{-1}) using a high pressure liquid chromatography (HPLC) pump (Scientific Systems) together with an inert sweep gas (pure N_2 at 40 sccm as controlled by a mass flow controller from Brooks Instrument) into a pre-heated (200 °C) mixing zone upstream of the reactor bed to vaporize the solution mixtures prior to encountering the catalyst bed. Monomer feed acid concentrations were selected based upon water solubility limits at room temperature due to equipment which limited feeds to room temperature; solubility increases non-linearly, thus different processes could investigate various feed solutions. Catalysts were packed in a 16.5″ long, 0.5″ outer diameter 316 stainless steel tube with an inert coating (SilcoTek) on the internal surface, where packing was kept within an isothermal zone in the tube (identified between 8.5″ and 11.5″ of the tube) with the remainder void filled with 1 mm borosilicate glass beads (Millipore Sigma) and ends plugged with quartz wool (Acros Organics). Temperature was monitored using an internal thermocouple centered within the isothermal zone and heated using a clam-shell ceramic furnace (Verder Scientific) enclosed around the tube, and reaction temperature was regulated using a PID controller (Opto 22).

Following preliminary tests, a reaction temperature of 350 °C was selected for experiments conducted in this study (only minor variations in 3HB conversion and propylene carbon selectivity observed for 325–375 °C as shown in Fig. S2†). System pressure was controlled using a piston-sensing backpressure regulator (Swagelok). The post-reaction product stream was cooled using a tube-in-tube heat exchanger and then separated with a stainless-steel vapor–liquid separator (Parr Instruments). The aqueous byproduct stream was collected using a bottom drain valve fitted on the vapor–liquid separator for analysis. Volumetric flow of the gaseous stream was measured using a gas flow calibrator (Mesa Labs) and gas samples were collected for analysis in ALTEF gas sampling bags (Restek). Propylene was quantified by gas chromatography with flame ionization detector (GC-FID – Thermo Fisher Scientific Trace 1310 GC with an FID and a Restek Alumina BOND/MAPD column), and CO_2 was quantified by GC with thermal conductivity detector (GC-TCD – Thermo Fisher Scientific Trace 1310 GC with a TCD and a Supelco Carboxen® 1010 PLOT column). Aqueous-soluble products were analyzed *via* HPLC with photodiode array detector (HPLC-PDA – Shimadzu Prominence system with a Waters Spherisorb® ODS2 column). Propylene and CO_2 reference standards were acquired from General Air. Reference standards for 3HB, CA, and acetaldehyde were obtained from Sigma-Aldrich, and acetic acid was obtained from Fluka.

Catalyst characterization

Catalysts were characterized by a variety of techniques. Specific surface area (m^2 g^{-1}), total pore volume (cm^3 g^{-1}), and average pore diameter (nm) were determined using N_2 physisorption. Samples were first degassed at 250 °C overnight under vacuum (virgin catalysts) or helium (spent catalysts) on a Quantachrome Quadrasorb SI. The Brunauer–Emmett–Teller (BET) method was applied to the N_2 physisorption data to calculate specific surface areas, and the Barrett–Joyner–Halenda (BJH) method was applied to calculate pore volumes and pore diameters.

Total acid site density (μmol g^{-1}) was measured by ammonia temperature programmed desorption (TPD) using a Micromeritics AutoChem 2920 Chemisorption Analyzer. Silica and alumina based samples were heated to 750 °C at 10 °C min^{-1} in He flowing at 60 sccm and held for 2 h for catalyst pretreatment. The temperature was reduced to 250 °C, and the samples were flushed with He for 10 min. For NH_3 treatment, 1.67% NH_3/He (v/v) was passed over the sample at 60 sccm for 5 min, then 8.33% NH_3/He flowed over the sample at 60 sccm for 1 hour. 60 sccm He was passed over the sample for 90 min to flush excess ammonia. The samples were heated to 750 °C in 30 sccm He at 5 °C min^{-1}, holding at 750 °C for 90 min. The released gas was measured with a thermal conductivity detector. The niobium-based catalysts were measured using a similar process with lower temperatures. The catalysts were pretreated at 500 °C at 10 °C min^{-1} in He flowing at 60 sccm for 3 h, followed by cooling to 120 °C before passing 10% NH_3/He over the catalyst for 1 h. The excess ammonia was flushed for 2 h with helium, before ramping to 500 °C in 50 sccm He at 10 °C min^{-1}, holding at 500 °C for 90 min.

The relative ratio of Brønsted to Lewis acid sites for silica–alumina and alumina catalysts was determined by pyridine adsorption diffuse reflectance Fourier transform infrared spectroscopy (py-DRIFTS), using a method adapted from a recent report.[47] Spectra represent the average of 64 scans collected at 4 cm^{-1} resolution using a Thermo Nicolet iS50 FT-IR spectrometer equipped with a Harrick Praying Mantis reaction chamber. Samples were pretreated under flowing N_2 at 10 °C min^{-1} to 450 °C and then held at this temperature for 1 h. After cooling to 150 °C at 10 °C min^{-1}, the samples

were purged with N_2 for 10 min, and a background spectrum was collected. The samples were then exposed to pyridine vapor for 10 min by flowing N_2 through a pyridine-filled bubbler held at room temperature. Physisorbed pyridine was subsequently desorbed in N_2 by heating to 200 °C at 10 °C min^{-1} and holding for 30 min. After cooling to 150 °C at 10 °C min^{-1}, a spectrum was collected and referenced to the background collected prior to pyridine exposure. The peak area of vibrational modes near 1445 cm^{-1} (Lewis) and 1540 cm^{-1} (Brønsted) were used to determine the relative ratio of Brønsted to Lewis acidic sites. The ratio of Brønsted to Lewis acid sites for niobium catalysts was previously published for the same batches of niobic acid and niobium phosphate using the same technique and instrument.[46]

Carbon contents of used SIAL 3113 and NbP was determined using a LECO CHN 628 elemental analyzer. NbP samples were analyzed in triplicate. SIAL 3113 was only analyzed once due to limited available sample mass.

Catalyst stability and deactivation

Separate experiments were conducted to evaluate the stability and deactivation of SIAL 3113 and NbP catalysts. First, partial conversion experiments were performed to monitor changes in catalyst activity that would not be observed if excess catalyst was present under complete conversion conditions. NbP and SIAL 3113 were evaluated using a CA feed with reaction conditions modified from the usual 6 h conversion experiments by decreasing catalyst mass and increasing feed CA concentration to adjust the WHSV from 0.1 to 2.66 h^{-1}. After continuous reaction with CA for 48 h time on stream, the used NbP was recovered from the reactor bed and re-calcined under air in a static muffle furnace (500 °C for 3 h; 200 °C h^{-1} heat rate), before placing back into the reactor and monitoring reaction with CA for an additional 10 h.

SIAL 3113 and Nb were also subjected to continuous 3HB feeds for 70 h with identical conditions to the 6 h experiments, collecting samples for analysis approximately every 8 h, focusing on trends in yields of the target propylene product. Catalysts were then removed from the reactor and subjected to N_2 physisorption analysis. The SIAL 3113 was then re-calcined under air in a static muffle furnace (550 °C for 3 h; 200 °C h^{-1} heat rate) to remove visible signs of carbonaceous deposits. The re-calcined SIAL 3113 was then tested under similar conditions to compare with the virgin catalyst. The effects of extended exposure to superheated water vapor alone on catalyst activity was also evaluated. SIAL 3113 and NbP were packed into the reactor and exposed to a deionized water feed (no monomer acid added) in the same manner described in Flow reactor experiments and product analysis for 66 h before introducing 3HB for 6 h and monitoring conversion reactions as described above. Specific surface area and porosity of the steam-exposed catalysts was also measured to compare with virgin and 3HB-reacted materials.

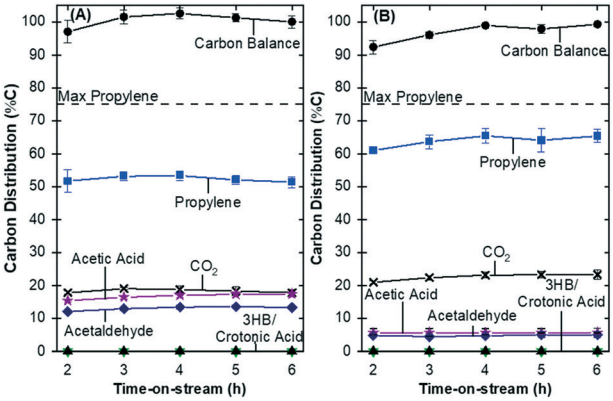

Fig. 2 Carbon selectivity (as %C of inflow 3HB feed) results for (A) 3HB and (B) CA conversion over SIAL 3113 over 6 h continuous time-on-stream measurement. Reaction conditions: 350 °C, 0.1 h^{-1} WHSV of 3HB, 40 sccm N_2 at 55 psig (gaseous products sampled at atmospheric pressure). Data points with error bars show the mean of duplicate reactions with min/max values where duplicates were performed (up to 4 h for (B)). Horizontal dotted line indicates theoretical maximum yield of propylene from conversion of 3HB.

Results and discussion

Vapor-phase catalytic reactions of 3HB and CA

Continuous time-on-stream measurements of 3HB aqueous feeds were conducted with SIAL 3113 packed into the reactor's catalyst bed. Complete conversion of 3HB was observed throughout the 6 h time-on-stream experiment; Fig. 2A shows the complete distribution of conversion products observed. Measured products are shown at %C distribution values,

$$\%C_i = \frac{n_i y_i}{n_{3HB,feed} \times y_{3HB}}(100\%)$$

where n_i is the moles min^{-1} of product "i" produced, y_i is the number of carbon atoms in the structure of "i", $n_{3HB,feed}$ is the moles min^{-1} of 3HB in the feed solution, and y_{3HB} = 4. This approach allows for a summation of products %C to determine overall carbon mass balances. Using this measure, complete conversion of 3HB was observed throughout the experiment, with propylene yields ranging from 51–53 %C and approximately equimolar concentrations of CO_2 (*i.e.*, 18–19 %C), in agreement with expectations for the pathway depicted in Fig. 1. Because the target product propylene contains one fewer carbon atom than 3HB, complete molar conversion of 3HB to propylene would yield %C of 75%, so the measured 51–53 %C for propylene indicates that 68–71% of the 3HB molecules in the feed solution were converted to the target product. Measurements show that the remainder of the 3HB in the feed was converted to other non-target products. Analysis showed that the remaining carbon balance (27–31 %C) could be accounted for by production of acetic acid and acetaldehyde, with overall carbon mass balances varying from 97–103% for the duration of the experiment.

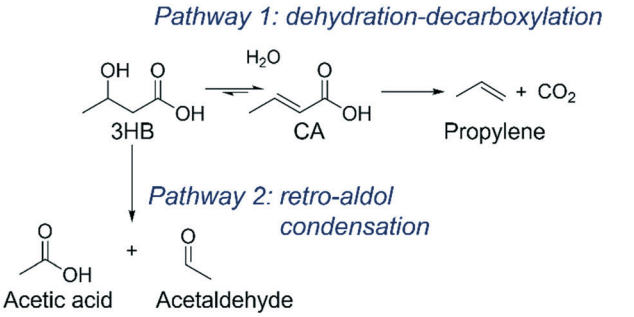

Scheme 1 Vapor-phase conversion of 3HB and CA over solid acid catalysts.

The observed products with SIAL 3113 (and other solid acid catalysts discussed below) are consistent with a reaction network shown in Scheme 1 involving two competing reaction pathways. The desired pathway leading to propylene and CO_2 (pathway 1) is consistent with a 2-step dehydration–decarboxylation (DHYD–DCBX) reactions with crotonic acid as an intermediate resulting from the initial dehydration of 3HB. In competition with this pathway is the retro-aldol conversion of 3HB to mixture of acetaldehyde and acetic acid (pathway 2).[48] A small molar excess of acetic acid is detected (average [acetic acid]:[acetaldehyde] = 1.4:1), attributed to partial oxidation of the latter under vapor-phase conditions.

Experiments performed without catalysts packed in the reaction tube (*i.e.*, a "blank" reaction; ESI† Fig. S3) showed near-identical yields of acetic acid/acetaldehyde as compared to results observed for SIAL 3113, indicating that the retro-aldol reaction occurs thermally upon heating and/or vaporizing the aqueous 3HB feed solution. Partial conversion of 3HB to CA was also observed in the absence of catalyst, indicating that heating/vaporization of the aqueous 3HB feed contributes to 3HB dehydration. Although catalyst-free controls were not performed with CA feeds, the lower yields of retro-aldol products observed in experiments with catalyst compared to experiments conducted with 3HB feeds is consistent with greater thermal stability of the former. According to Scheme 1, CA and 3HB can interconvert *via* a reversible hydration/dehydration reaction, with the latter being subject to retro-aldol conversion. Thus, future work is recommended to examine in detail the factors controlling CA hydration and decarboxylation reactions.

Separate experiments with SIAL 3113 were also carried out using CA as the aqueous feedstock in place of 3HB (Fig. 2B). In comparison to 3HB, reaction of CA yielded increased propylene (61–65 %C) and a corresponding decrease in formation of the retro-aldol products (9.5–12.5 %C). This is consistent with the greater thermal stability of CA over 3HB within the superheated steam matrix, and results in a slightly higher propylene yield than comparable thermolysis experiments.[18] A mixture of CA and 3HB acid monomers are typically produced upon depolymerization of PHB, so facile conversion of both monomer acids to propylene is ideal for this process.

The pathways depicted in Scheme 1 are also supported by previous studies reporting acetic acid and acetaldehyde production during conversion of γ-valerolactone (GVL) over γ-Al_2O_3,[49] where the authors attributed the retro-aldol reaction to catalysis resulting from the basicity of γ-Al_2O_3. Interestingly, negligible quantities of these products were observed when γ-valerolactone or 3-butenoic acid (a vinyl analog of CA) were reacted over SIAL 3113.[50] The fact that acetic acid/acetaldehyde yields with 3HB were largely insensitive to the presence/absence of SIAL 3113 indicates that this reaction is more thermochemical, than catalytic, in nature. This conclusion is further supported by a small increase in the observed yields of retro-aldol products when increasing reaction temperature from 325 °C (32 %C) to 375 °C (38 %C) (Fig. S2†). No evidence of further decarboxylation of acetic acid by the catalysts was observed during experiments, consistent with prior reports showing high rates of acid-catalyzed decarboxylation of unsaturated carboxylic acids in comparison to their saturated analogues.[50]

Ultimately, further work is needed to fully elucidate the conditions controlling retro-aldol reaction product yields – including differences in feedstock, concentration in water, as well as other operational factors (*e.g.*, sweep gas flow rate, pre-heat vaporization temperature, system pressure) – with a goal of reducing carbon lost to this pathway. Additional research is needed to evaluate recovering carbon by recycling retro-aldol products as a substrate for PHB-producing microbes. PHB-accumulating organisms frequently use VFAs as a substrate,[9,10] and recent research has shown engineered PHA-accumulating microbes can survive and utilize toxic acetaldehyde.[51] This finding also highlights the need for further catalyst design work to reduce barriers to the preferred dehydration–decarboxylation pathway and optimize operation conditions.

Reaction of 3HB with other solid acid catalysts

Experiments with 3HB feed solutions similar to those shown in Fig. 2 with SIAL 3113 were conducted with a series of silica–alumina, alumina, and niobium solid acid catalysts possessing varying surface and acidic properties (*e.g.*, varying Brønsted *versus* Lewis acidities, specific surface areas) (Table 1). Fig. 3A shows time-dependent propylene yields observed when the flow reactor was packed with each of the catalysts (full product distributions for each of the catalysts is provided in Fig. S4†). These results show widely varying propylene yields among the catalysts. The highest yields were observed for SIAL 3113 and NbP (%C_{avg} values of 53 and 54 %C, respectively, after 4 h time on stream), followed by SIAL 3125 (37 %C) and NbO (21 %C). For NbP, propylene yields climbed throughout the 6 h time-on-stream experiment, growing from 46 %C in samples collected after 2 h to values ranging from 51–59 %C for samples collected from 3–6 h. As discussed later, similar growth in yields was observed over the first few hours of 3HB feed following extended exposure to steam only. Similar induction periods for bulk niobium

Table 1 Virgin solid acid catalyst characteristics

Catalyst	Brønsted acid sites (μmol g^{-1})	Lewis acid sites (μmol g^{-1})	Specific surface area (m^2 g^{-1})	Pore volume (cm^3 g^{-1})	Pore diameter (nm)
SIAL 3113[a]	202	495	565	0.85	4.4
SIAL 3125[a]	93	301	409	0.75	5.0
γ-Al_2O_3[a]	0	311	214	0.51	6.3
Na-SIAL 3113[a]	0	134[c]	159	0.83	17.6
NbP[b]	270[d]	68[d]	130	0.35	3.7
NbO[b]	19[d]	132[d]	66	0.15	3.1

[a] Pretreatment: calcined in air for 3 hours at 450 °C (200 °C h^{-1} heat-up rate). [b] Pretreatment: calcined in air for 3 hours at 400 °C (200 °C h^{-1} heat-up rate). [c] Reduction in Lewis acid sites in Na-SIAL 3113 assumed to result from blockage of selected pores due to adsorption of sodium ions, consistent with the reduction in BET specific surface area and increase in average pore diameter. [d] Calculated using DRIFTS data from Hafenstine *et al.*[46]

oxides have been reported previously.[42,52] The lowest yield for a virgin catalyst was observed for γ-Al_2O_3 (17 %C). Full product analysis showed complete disappearance of 3HB with all the catalysts, with the same analytes being detected that were described for SIAL 3113. It follows, then, that differences between the catalysts result from varying activities for further conversion of CA to propylene/CO_2 *versus* the retro-aldol products.

Analysis of the observed trends in production of the target propylene product reveal the importance of Brønsted acid site density. The two solid acid catalysts where the highest propylene yields were observed (NbP and SIAL3113) have, by a large margin, the highest density of Brønsted acid sites, and Fig. 3B shows the relationship between Brønsted acid site density and propylene yield for the full set of solid acid catalysts tested. In comparison, none of the other characteristics appear to correlate with activity. In particular, the specific surface area, pore volume, and Lewis acid site density for NbP are among the lowest of the solid acid catalysts tested. Furthermore, the surface area and pore characteristics of virgin SIAL 3113, SIAL 3125, and γ-Al_2O_3 were similar, suggesting that physical surface properties are less likely to be responsible for the differences in propylene yields observed between these three catalysts. Finally, tests conducted with SIAL 3113 after pre-treatment with excess Na^+ to poison the Brønsted sites[44] (referred to hereafter as Na-SIAL 3113) showed the lowest propylene yield (11–13 %C) of all the catalysts tested. Interestingly, yields of the retro-aldol reaction products observed for SIAL 3125 and Na-SIAL 3113 (Fig. S4†) were fairly similar to those observed for the more highly active SIAL 3113 and NbP catalysts, consistent with the conclusion that this reaction is more thermochemical than catalytic in nature. Increased yields of the retro-aldol products were observed with γ-Al_2O_3 (28 %C as acetaldehyde and 35 %C as acetic acid after 4 h time-on-stream), which may result from the material's basicity, as reported previously for γ-valerolactone.[49] For NbO, similar yields of acetaldehyde were observed as for the silica–alumina and NbP catalysts, but acetic acid yields were significantly increased. Thus, it is unclear if this material is catalyzing the retro-aldol pathway or if the additional acetic acid was formed through a different pathway such as the limited redox properties of bulk niobium oxide.[53]

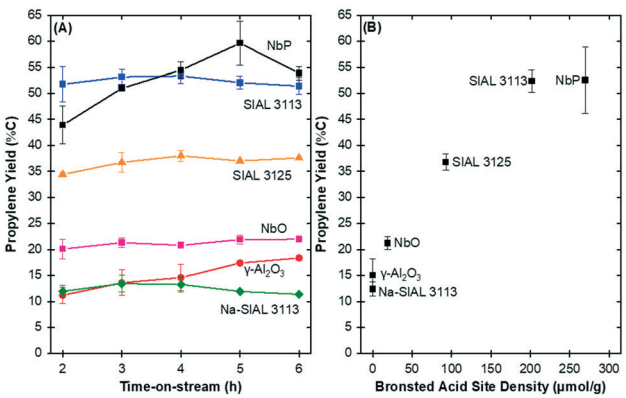

Fig. 3 (A) Propylene carbon selectivity (as %C of inflow 3HB feed) results for time-on-stream vapor-phase reactions of 3HB over different solid acid catalysts listed in Table 1. (B) Relationship between the Brønsted acid site densities and propylene yields observed after 4 h time-on-stream with different solid acid catalysts. Reaction conditions: 350 °C, 0.1 h^{-1} WHSV, 40 sccm N_2 at 55 psig (gaseous products sampled at atmospheric pressure). Data points with error bars show the mean of duplicate reactions with min/max values where duplicates were performed. Full product distributions for the same experimental runs are provided in Fig. S4.†

Given the high propylene yields observed for 3HB reactions with NbP, a time-on-stream experiment was also conducted with CA feed solution. Results of this experiment (Fig. S5†) are almost identical to those discussed for SIAL 3113 in Fig. 2, showing propylene yields ranging from 59–63 %C throughout the time-on-stream experiment. This confirms the material's mode of activity and supporting its further examination as an alternative to the silica–alumina material.

Preference for Brønsted acidity in promoting dehydration and decarboxylation reactions have previously been observed for a number of vapor-phase reactions (*e.g.*, γ-valerolactone conversion to butenes;[49] glycerol conversion to acrolein;[44] and dehydration of 2-butanol[54]). In contrast, Lewis acidity is favored for isomerization of longer-chain alkene products to linear alpha olefins at the expense of overall alkene yields (*e.g.*, conversion of γ-valerolactone specifically to 1-butene isomer over γ-Al_2O_3 with 43% total butene yields and 92%

selectivity for 1-butene among all isomers). Although the trade-offs between Brønsted and Lewis acidity do not appear to be immediately relevant for dehydration–decarboxylation of 3HB given that the alkene product (*i.e.*, propylene) has no isomers with regards to the position of the double bond, achieving a high density of Brønsted acidic sites might require the presence of alumina in the amorphous silica–alumina catalysts (*i.e.*, the presence of aluminum near the silanol groups is thought to promote Brønsted acidity),[35,55] which simultaneously provides Lewis acidity in the same materials.

Catalyst stability and deactivation

Following the promising activity observed with SIAL 3113 and NbP catalysts, further experiments were undertaken to assess their stability and potential for deactivation during longer-term operation. Extended time-on-stream experiments were conducted with modified conditions where only partial monomer acid conversion would be observed with the virgin catalysts (the WHSV was increased from 0.1 to 2.75 h^{-1}). Furthermore, we switched to a CA feed solution to simplify analysis, since much of the initial 3HB to CA conversion occurs thermochemically rather than catalytically, and because NbP does not undergo an induction period when exposed to CA (Fig. S5†). Fig. 4 shows the results of this experiment for both SIAL 3113 and NbP. First, it is interesting to note that the increase in WHSV led to much larger reduction in CA-to-propylene yields for virgin SIAL 3113 (reduced from 64 to 20 %C) than from NbP (reduced from 63 to 37 %C) (full product distributions are shown in Fig. S6†). Thus, on a mass basis, NbP provides nearly twice as much activity for CA conversion to propylene as SIAL 3113, a fact that was masked in results observed during the 6 h experiments where full conversion of 3HB was observed with both materials. The experiment using SIAL 3113 showed continuous decreases in propylene yield with extended time-on-stream, decreasing from 20 to 5 %C after 48 h of continuous operation. We also observed a reduction in propylene yield from CA over time when using the NbP catalyst, decreasing from 37 to 17 C% over 48 h of continuous reaction.

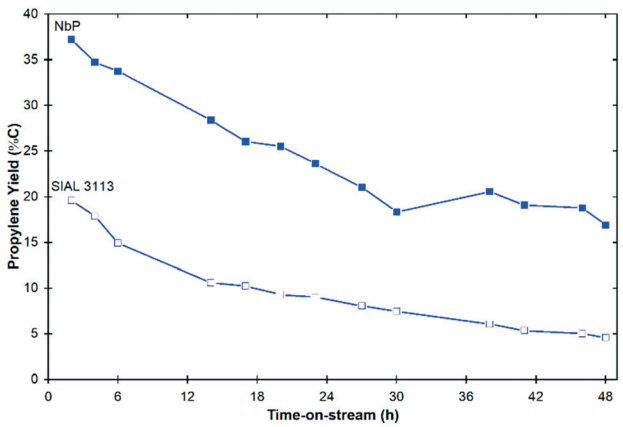

Fig. 4 Partial conversion of CA to propylene over NbP (filled markers) and SIAL 3113 (unfilled markers). Reaction conditions: 350 °C, 2.75 h^{-1} WHSV, 40 sccm N_2 at 55 psig. Full conversion and product distribution data provided in Fig. S6 in ESI.†

While data in Fig. 3B is suggestive of a link between Brønsted acid site density and rates of acid conversion to propylene, the specific mode of action may be more complex (*e.g.*, involving cooperative action between Brønsted and Lewis acid sites). Direct correlation between catalytic activity and Brønsted acid site density is further complicated by the effects of catalyst surface hydration upon exposure to the water vapor stream that is not accounted for by acid site characterization techniques performed under anhydrous conditions. For example, the 2-fold higher specific mass activity of NbP for CA-to-propylene compared to SIAL 3113 could be explained by greater increases in Brønsted acidity of the former under *in situ* conditions. This is consistent with previous reports showing increases in acidity and activity of Nb-based catalysts upon exposure to water vapor streams.[56,57] Conflicting reports on the effects of water vapor on surface acidity of amorphous silica–alumina catalysts have also been noted, with some authors finding increases in Brønsted acid sites,[58,59] while others observed no effects.[60]

The nature of this deactivation was further probed by characterizing SIAL 3113 and NbP exposed to continuous 3HB feeds and superheated steam. SIAL 3113 and NbP were recovered after continuously processing 3HB for 70 h under the same experimental conditions as the previously described 6 h experiments (full product distribution in Fig. S7†). N_2 physisorption results (Table 2) reveal a large loss in specific surface area for SIAL 3113 (from 565 to 344 $m^2\ g^{-1}$) and NbP (130 to 60 $m^2\ g^{-1}$). In addition, a noticeable color change was observed between the virgin catalysts and the material recovered from the reactor after 70 h time-on-stream. This is similar to previous reports with GVL,[36] and is suggestive of the formation of coking deposits that can contribute to catalyst deactivation.

The loss of surface area was accompanied by a loss of propylene production for SIAL 3113, with yields dropping continuously from an average of 52 %C over the first 6 h of reaction to 42 %C after 42 h and further to 40 %C after 70 h. Corresponding increases in residual CA were observed over the same time period, suggesting a loss in active sites that promote decarboxylation since dehydration of 3HB to CA occurs largely by thermochemical means prior to exposure to the catalyst (see catalyst-free blank reaction shown in Fig. S2†). In comparison NbP retained propylene yields from 3HB for the duration of the 70 h experiment. Propylene yields remained high throughout (51.5 ± 4.0 %C (av ± SD) for 12–70 h *versus* 52.5 ± 6.4 %C for 0–6 h), and no CA intermediate was observed in any of the samples collected for analysis throughout the experiment (Fig. S7b†). While promising, these results do not prove long-term NbP stability, because the superior performance of NbP can mask deactivation.

Table 2 Virgin, spent, re-calcined, and vapor-exposed catalyst characteristics of SIAL 3113 and NbP

		Specific surface area (m^2 g^{-1})	Pore volume (cm^3 g^{-1})	Pore diameter (nm)	%C
SIAL 3113	Virgin	565	0.85	4.4	0.00
	After 70 h reaction[a]	344	0.78	5.7	0.42
	Re-calcined	332	0.78	5.7	0.06
	Vapor-exposed[b]	345	0.79	5.6	0.16
NbP	Virgin	130	0.30	3.7	0.03
	After 70 h reaction[a]	60	0.30	3.7	1.76
	Re-calcined	73	0.34	3.7	0.04
	Vapor-exposed[b]	60	0.32	11.4	0.70

[a] After 70 h time-on-stream reaction with 3HB, see Fig. S7.† [b] After 66 h time-on-stream exposure to superheated water vapor (350 °C, 55 psig) at 0.3 mL min^{-1}, followed by 6 h time-on-stream reaction with 3HB; see Catalyst characterization for details. Reaction conditions: 350 °C, 0.1 h^{-1} WHSV of 3HB, 40 sccm N_2 at 55 psig (gaseous products sampled at atmospheric pressure).

Follow-up experiments showed that these changes were induced principally by extended exposure to the superheated water vapor, rather than the 3HB in the same feed. Re-calcination of the recovered catalysts from the 70 h experiment caused a restoration of most of the original catalyst color, but led to decreased surface area for SIAL 3113 (from 344 to 332 m^2 g^{-1}), and only provided limited recovery for NbP (from 60 to 73 m^2 g^{-1}). Following an additional 6 h reaction, the re-calcined SIAL 3113 exhibited no improvement in propylene yields (Fig. S7a†). NbP could not be tested in the same way, as there was no evidence of decreased catalyst activity in the 70 h experiment. Thus, it appears that deactivation was linked more to irreversible physical changes induced in the catalyst than blocking of surface sites by coke deposits. Similar reductions in specific surface area of SIAL 3113 and NbP (Table 2) were observed when the catalysts were exposed to a stream of superheated water vapor alone for 66 h prior to introducing 3HB into the feedwater. Following the introduction of 3HB to the catalysts exposed to superheated water vapor, SIAL 3113 deactivation was observed to a level similar to that observed following extended reaction with 3HB, whereas the reaction catalyzed by NbP showed similar propylene yields as the virgin catalyst (Fig. S8†).

Deactivation attributed to physical catalyst changes was further supported by the quantity of carbon on the spent catalysts. Re-calcination of SIAL 3113 exposed to 3HB for 70 h showed a reduction of carbon on the surface from 0.42% to 0.06% of the total recovered catalyst mass, with no recovery in performance. NbP retained 4 times more carbon by mass (1.76%) than SIAL 3113, yet saw no decrease in performance.

We also speculate that deactivation is related to decreasing availability of Brønsted acid sites after extended time-on-stream. Unfortunately, coking deposits that are visually apparent on the deactivated catalysts interfere with NH_3-TPD measurements for total acidity and the py-DRIFTS method for characterizing the relative ratio of Brønsted to Lewis acid sites. Following recalcination, total acid site density for SIAL 3113 decreased from 697 (virgin catalyst) to 607 μmol g^{-1}, but residual discoloration of the material would continue to interfere with the py-DRIFTS measurements.

The findings described above are consistent with some past reports documenting instability of mesoporous silica–alumina catalysts exposed to superheated steam environments.[40,61] The loss in surface area of SIAL 3113 is consistent with sintering that can damage the material's porous physical structure.[62,63] This can also lead to de-alumination of the SIAL catalyst, wherein aluminum separates from the silica–alumina framework, thereby altering acidic properties of the material surface. Further study of Al and Si spatial distribution within the material framework is needed to elucidate the major mechanisms responsible for catalyst deactivation during vapor-phase processing of 3HB. Previous work examining GVL reactions over solid acid catalysts suggested coke deposition as a major mechanism for catalyst deactivation,[36,45] with qualitative claims of activity restoration of the catalysts upon re-calcination to restore color (*i.e.*, no results were shown for tests with re-calcined catalysts).[17,45] However, these studies were conducted with much more concentrated organic feed solutions (20–30 wt% in water *versus* 2 wt% in this study) where rapid coke deposition is more favorable.

As re-calcined NbP performance could not be tested in the same manner as SIAL 3113 due to complete CA conversion, NbP recovered from the 48 h partial conversion of CA experiment was re-calcined and reintroduced to the CA feed. Following re-calcination of NbP, propylene yields increased from 17 to 28 %C (compared to 37 %C for virgin catalyst), showing that performance of NbP can be partially recovered following re-calcination, unlike that of SIAL 3113. The conclusion that NbP deactivation was caused principally by coke deposition is supported by the CHN measurements (Table 1) showing increases in carbon content of the solid following 70 h time-on-stream (from 0.03 to 1.76 %C). Thus, NbP retains more carbon on the surface than SIAL 3113, nearly all of which could be removed through re-calcination (from 1.76% back to 0.04% following re-calcination, compared to 0.03% of the virgin catalyst). This, accompanied by the decrease in surface area in spent NbP which is not accompanied by decreased performance supports the conclusion that overall specific surface area is not a major controlling factor in the catalyst's reactivity with the monomer acids, and that the measurable physical

characteristics of the catalyst may not entirely explain the catalyst functionality. Continued measurements for 10 h show that deactivation continued after re-calcination. Although these findings indicate that deactivation of NbP cannot be avoided during vapor-phase reactions with the monomer acids, and recovery of catalyst activity by re-calcination was incomplete, they suggest a strategy for sustained catalyst operation *via* periodic catalyst regeneration. Further research is needed to optimize the re-calcination process and regeneration frequency for NbP to sustain monomer acid conversions.

Conclusions

Results of continuous on-stream vapor-phase processing of aqueous 3HB and CA monomer acid feeds demonstrate facile production of propylene, a valuable feedstock for industrial production of chemicals and liquid hydrocarbon fuels. Propylene results from dehydration and decarboxylation reactions catalyzed by silica–alumina and niobium-based solid acid catalysts. Comparison among catalysts highlights the importance of Brønsted acidity in promoting the desired reaction pathway. Undesirable formation of C2 products (acetic acid and acetaldehyde) *via* retro-aldol conversion occurs in both the presence and absence of catalysts and is attributed principally to thermochemical instability of the monomer acids in the superheated vapor matrix. Extended time-on-stream experiments show that SIAL 3113 experiences slow, but irreversible, catalyst deactivation due to steam-induced changes in catalyst structure, including decreases in surface area. NbP also shows a decrease in surface area. However, no detectable decrease in propylene formation from 3HB was observed over 70 h time-on-stream. Experiments with CA shown some deactivation of NbP, but this was partially reversible by re-calcination, suggesting greater thermal and aqueous stability. Further research is recommended to limit NbP deactivation and sustain conversion of PHB-derived monomer acids. This finding provides a path forward for production of propylene and associated high value products from wastewater organic carbon *via* integrated funneling of carbon to intracellular polyhydroxybutyrate and subsequent separation, depolymerization and catalytic conversion with Nb-based acid catalysts. Further work is needed to elucidate the controlling mechanisms responsible for the desired and non-target conversion reactions, and to optimize catalyst regeneration conditions and timing to sustain long-term operation of catalytic reactor systems.

Conflicts of interest

There are no conflicts to declare.

Acknowledgements

Financial support for this work was provided by the National Science Foundation (NSF) through the NSF Engineering Research Center for Reinventing the Nation's Urban Water Infrastructure Systems (ReNUWIt; EEC-1028968), a grant from the Colorado Higher Education Competitive Research Authority (CHECRA), and NSF Award CBET-1804513. Support for AK was provided by a joint CSM-NREL Energy Fellowship and the NSF Graduate Research Fellowship Program (DGE-1646713). Support for SL was provided by the National Research Foundation Singapore under its National Research Foundation (NRF) Environmental and Water Technologies (EWT) PhD Scholarship Programme and administered by the Environment and Water Industry Programme Office (EWI). Work at NREL was supported by the U.S. Department of Energy under Contract No. DEAC36-08GO28308 with the National Renewable Energy Laboratory. The authors wish to thank Davis Conklin (NREL) for valuable discussion on catalyst characterization, Jim Stunkel (NREL) for valuable input on flow reaction experiments, and Rianna Martinez (NREL) for CHN analysis. The views and opinions of the authors expressed herein do not necessarily state or reflect those of the United States Government or any agency thereof. Neither the United States Government nor any agency thereof, nor any of their employees, makes any warranty, expressed or implied, or assumes any legal liability or responsibility for the accuracy, completeness, or usefulness of any information, apparatus, product, or process disclosed, or represents that its use would not infringe privately owned rights.

Notes and references

1 M. C. M. van Loosdrecht and D. Brdjanovic, *Science*, 2014, **344**, 1452–1453.
2 J. S. Guest, S. J. Skerlos, J. L. Barnard, M. B. Beck, G. T. Daigger, H. Hilger, S. J. Jackson, K. Karvazy, L. Kelly, L. Macpherson, J. R. Mihelcic, A. Pramanik, L. Raskin, M. C. M. Van Loosdrecht, D. Yeh and N. G. Love, *Environ. Sci. Technol.*, 2009, **43**, 6126–6130.
3 S. Leow, B. D. Shoener, Y. Li, J. L. DeBellis, J. Markham, R. Davis, L. M. L. Laurens, P. T. Pienkos, S. M. Cook, T. J. Strathmann and J. S. Guest, *Environ. Sci. Technol.*, 2018, **52**, 13591–13599.
4 Y. Li, S. Leow, T. Dong, N. J. Nagle, E. P. Knoshaug, L. M. L. Laurens, P. T. Pienkos, J. S. Guest and T. J. Strathmann, *ACS Sustainable Chem. Eng.*, 2019, **7**, 5835–5844.
5 J. G. Linger, D. R. Vardon, M. T. Guarnieri, E. M. Karp, G. B. Hunsinger, M. A. Franden, C. W. Johnson, G. Chupka, T. J. Strathmann, P. T. Pienkos and G. T. Beckham, *Proc. Natl. Acad. Sci. U. S. A.*, 2014, **111**, 12013–12018.
6 D. R. Vardon, M. Ann Franden, C. W. Johnson, E. M. Karp, M. T. Guarnieri, J. G. Linger, M. J. Salm, T. J. Strathmann and G. T. Beckham, *Energy Environ. Sci.*, 2015, **8**, 617–628.
7 M. Suresh Kumar, S. N. Mudliar, K. M. K. Reddy and T. Chakrabarti, *Bioresour. Technol.*, 2004, **95**, 327–330.
8 E. Korkakaki, M. Mulders, A. Veeken, R. Rozendal, M. C. M. van Loosdrecht and R. Kleerebezem, *Water Res.*, 2016, **96**, 74–83.

9 J. Tamis, K. Lužkov, Y. Jiang, M. C. M. van Loosdrecht and R. Kleerebezem, *J. Biotechnol.*, 2014, **192**, 161–169.
10 S. Bengtsson, A. Werker, M. Christensson and T. Welander, *Bioresour. Technol.*, 2008, **99**, 509–516.
11 N. Basset, E. Katsou, N. Frison, S. Malamis, J. Dosta and F. Fatone, *Bioresour. Technol.*, 2016, **200**, 820–829.
12 S. Bengtsson, A. Karlsson, T. Alexandersson, L. Quadri, M. Hjort, P. Johansson, F. Morgan-Sagastume, S. Anterrieu, M. Arcos-Hernandez, L. Karabegovic, P. Magnusson and A. Werker, *New Biotechnol.*, 2017, **35**, 42–53.
13 F. Morgan-Sagastume, M. Hjort, D. Cirne, F. Gérardin, S. Lacroix, G. Gaval, L. Karabegovic, T. Alexandersson, P. Johansson, A. Karlsson, S. Bengtsson, M. V. Arcos-Hernández, P. Magnusson and A. Werker, *Bioresour. Technol.*, 2015, **181**, 78–89.
14 M. Koller, H. Niebelschütz and G. Braunegg, *Eng. Life Sci.*, 2013, **13**, 549–562.
15 M. H. Madkour, D. Heinrich, M. A. Alghamdi, I. I. Shabbaj and A. Steinbüchel, *Biomacromolecules*, 2013, **14**, 2963–2972.
16 C. Samorì, F. Abbondanzi, P. Galletti, L. Giorgini, L. Mazzocchetti, C. Torri and E. Tagliavini, *Bioresour. Technol.*, 2015, **189**, 195–202.
17 J. Q. Bond, D. M. Alonso, D. Wang, R. M. West and J. A. Dumesic, *Science*, 2010, **327**, 1110–1114.
18 J. M. Clark, H. M. Pilath, A. Mittal, W. E. Michener, D. J. Robichaud and D. K. Johnson, *J. Phys. Chem. A*, 2016, **120**, 332–345.
19 S. Kang, H. Chen, Y. Zheng, Y. Xiao, Y. Xu and Z. Wang, *ChemistrySelect*, 2019, **4**, 403–406.
20 S. Kang, X. Zhang, W. Zhang, W. Li, H. Chen, P. Yang, P. Tang, K. Cheng and Y. Xu, *Energy Fuels*, 2018, **32**, 11639–11644.
21 C. Fernández-Dacosta, J. A. Posada, R. Kleerebezem, M. C. Cuellar and A. Ramirez, *Bioresour. Technol.*, 2015, **185**, 368–377.
22 C. Fernández-Dacosta, J. A. Posada and A. Ramirez, *J. Cleaner Prod.*, 2016, **137**, 942–952.
23 C. Fernández-Dacosta, J. A. Posada, R. Kleerebezem, M. C. Cuellar and A. Ramirez, *Bioresour. Technol.*, 2015, **185**, 368–377.
24 X. J. Jiang, B. A. Ramsay and J. A. Ramsay, *Environ. Eng. Sci.*, 2014, **31**, 49–54.
25 Y. Li and T. J. Strathmann, *Green Chem.*, 2019, **21**, 5586–5597.
26 T. Saeki, T. Tsukegi, H. Tsuji, H. Daimon and K. Fujie, *Polymer*, 2005, **46**, 2157–2162.
27 C. R. Fischer, A. A. Peterson and J. W. Tester, *Ind. Eng. Chem. Res.*, 2011, **50**, 4420–4424.
28 C. Torri, T. D. O. Weme, C. Samorì, A. Kiwan and D. W. F. Brilman, *Environ. Sci. Technol.*, 2017, **51**, 12683–12691.
29 J. Q. Bond, C. S. Jungong and A. Chatzidimitriou, *J. Catal.*, 2016, **344**, 640–656.
30 M. Zabeti, W. M. A. Wan Daud and M. K. Aroua, *Fuel Process. Technol.*, 2009, **90**, 770–777.
31 G. W. Huber, R. D. Cortright and J. A. Dumesic, *Angew. Chem.*, 2004, **116**, 1575–1577.
32 W. Guan, C.-W. Tsang, C. S. K. Lin, C. Len, H. Hu and C. Liang, *Bioresour. Technol.*, 2020, **298**, 122432.
33 A. Corma and H. García, *Chem. Rev.*, 2003, **103**, 4307–4366.
34 S. van Donk, J. H. Bitter and K. P. de Jong, *Appl. Catal., A*, 2001, **212**, 97–116.
35 E. J. M. Hensen, D. G. Poduval, V. Degirmenci, D. A. J. M. Ligthart, W. Chen, F. Maugé, M. S. Rigutto and J. A. R. van Veen, *J. Phys. Chem. C*, 2012, **116**, 21416–21429.
36 A. B. Kellicutt, R. Salary, O. A. Abdelrahman and J. Q. Bond, *Catal. Sci. Technol.*, 2014, **4**, 2267–2279.
37 S. Kang, R. Miao, J. Guo and J. Fu, *Catal. Today*, 2021, **374**, 61–76.
38 I. Nowak and M. Ziolek, *Chem. Rev.*, 1999, **99**, 3603–3624.
39 K. Tanabe, *Catal. Today*, 2003, **78**, 65–77.
40 H. Xiong, H. N. Pham and A. K. Datye, *Green Chem.*, 2014, **16**, 4627–4643.
41 J. Huo, J.-P. Tessonnier and B. H. Shanks, *ACS Catal.*, 2021, **11**, 5248–5270.
42 K. Ogasawara, T. Iizuka and K. Tanabe, *Chem. Lett.*, 1984, **13**, 645–648.
43 P. Carniti, A. Gervasini, S. Biella and A. Auroux, *Chem. Mater.*, 2005, **17**, 6128–6136.
44 G. S. Foo, D. Wei, D. S. Sholl and C. Sievers, *ACS Catal.*, 2014, **4**, 3180–3192.
45 J. Q. Bond, D. Wang, D. M. Alonso and J. A. Dumesic, *J. Catal.*, 2011, **281**, 290–299.
46 G. R. Hafenstine, N. A. Huq, D. R. Conklin, M. R. Wiatrowski, X. Huo, Q. Guo, K. A. Unocic and D. R. Vardon, *Green Chem.*, 2020, **22**, 4463–4472.
47 X. Huo, N. A. Huq, J. Stunkel, N. S. Cleveland, A. K. Starace, A. E. Settle, A. M. York, R. S. Nelson, D. G. Brandner, L. Fouts, P. C. S. John, E. D. Christensen, J. Luecke, J. Hunter Mack, C. S. McEnally, P. A. Cherry, L. D. Pfefferle, T. J. Strathmann, D. Salvachúa, S. Kim, R. L. McCormick, G. T. Beckham and D. R. Vardon, *Green Chem.*, 2019, **21**, 5813–5827.
48 A. A. Marianou, C. C. Michailof, D. Ipsakis, K. Triantafyllidis and A. A. Lappas, *Green Chem.*, 2019, **21**, 6161–6178.
49 D. Wang, S. H. Hakim, D. M. Alonso and J. A. Dumesic, *Chem. Commun.*, 2013, **49**, 7040–7042.
50 J. Q. Bond, D. Martin Alonso, R. M. West and J. A. Dumesic, *Langmuir*, 2010, **26**, 16291–16298.
51 L. N. Jayakody, C. W. Johnson, J. M. Whitham, R. J. Giannone, B. A. Black, N. S. Cleveland, D. M. Klingeman, W. E. Michener, J. L. Olstad, D. R. Vardon, R. C. Brown, S. D. Brown, R. L. Hettich, A. M. Guss and G. T. Beckham, *Energy Environ. Sci.*, 2018, **11**, 1625–1638.
52 S.-H. Chai, H.-P. Wang, Y. Liang and B.-Q. Xu, *J. Catal.*, 2007, **250**, 342–349.
53 M. Ziolek, *Catal. Today*, 2003, **78**, 47–64.
54 R. M. West, D. J. Braden and J. A. Dumesic, *J. Catal.*, 2009, **262**, 134–143.
55 K. Larmier, C. Chizallet, S. Maury, N. Cadran, J. Abboud, A.-F. Lamic-Humblot, E. Marceau and H. Lauron-Pernot, *Angew. Chem., Int. Ed.*, 2017, **56**, 230–234.
56 K. Tanabe and S. Okazaki, *Appl. Catal., A*, 1995, **133**, 191–218.

57 S. Okazaki and N. Wada, *Catal. Today*, 1993, **16**, 349–359.
58 V. Sanchez Escribano, G. Garbarino, E. Finocchio and G. Busca, *Top. Catal.*, 2017, **60**, 1554–1564.
59 J. Blanchard, J.-M. Krafft, C. Dupont, C. Sayag, T. Takahashi and H. Yasuda, *Catal. Today*, 2014, **226**, 89–96.
60 E. Garrone, B. Onida, B. Bonelli, C. Busco and P. Ugliengo, *J. Phys. Chem. B*, 2006, **110**, 19087–19092.
61 D. E. Perea, I. Arslan, J. Liu, Z. Ristanović, L. Kovarik, B. W. Arey, J. A. Lercher, S. R. Bare and B. M. Weckhuysen, *Nat. Commun.*, 2015, **6**, 7589.
62 A. Corma, M. S. Grande, V. Gonzalez-Alfaro and A. V. Orchilles, *J. Catal.*, 1996, **159**, 375–382.
63 B. R. Johnson, N. L. Canfield, D. N. Tran, R. A. Dagle, X. S. Li, J. D. Holladay and Y. Wang, *Catal. Today*, 2007, **120**, 54–62.

Supplemental Information

for

Vapor-phase catalytic conversion of aqueous 3-hydroxybutyric acid and crotonic acid to propylene

Shijie Leow[a,b,d,e, †], Andrew J. Koehler[a,b,c, †], Lauren E. Cronmiller[a,b], Xiangchen Huo[a,c], Gabriella D. Lahti[c], Yalin Li[a,b,d], Glenn R. Hafenstine[c], Derek R. Vardon[c,*], Timothy J. Strathmann[a,*]

[a] Department of Civil and Environmental Engineering, Colorado School of Mines, 1500 Illinois St., Golden, CO 80401.

[b] Engineering Research Center for Re-inventing the Nation's Urban Water Infrastructure (ReNUWIt), Colorado School of Mines, Golden, Colorado 80401.

[c] National Renewable Energy Laboratory, 15013 Denver West Parkway, Golden, CO 80401.

[d] Department of Civil and Environmental Engineering, University of Illinois at Urbana-Champaign. Newmark Civil Engineering Laboratory, 205 N. Mathews Ave., Urbana, IL 61801.

[e] Current Affiliation: Nanyang Technological University, Nanyang Environment & Water Research Institute, 1 Cleantech Loop, CleanTech One, #06-08, 637141, Singapore

[†] Authors contributed equally

* Corresponding Authors: Timothy J. Strathmann. Department of Civil and Environmental Engineering, Colorado School of Mines, 1500 Illinois St., Golden, CO 80401. Telephone: (303) 384-2226, Email: strthmnn@mines.edu; Derek R. Vardon, National Bioenergy Center, National Renewable Energy Laboratory. 15013 Denver West Parkway, Golden, CO 80401. Telephone: (303) 384-7763; derek.vardon@nrel.gov

June 2021

8 Pages

8 Figures

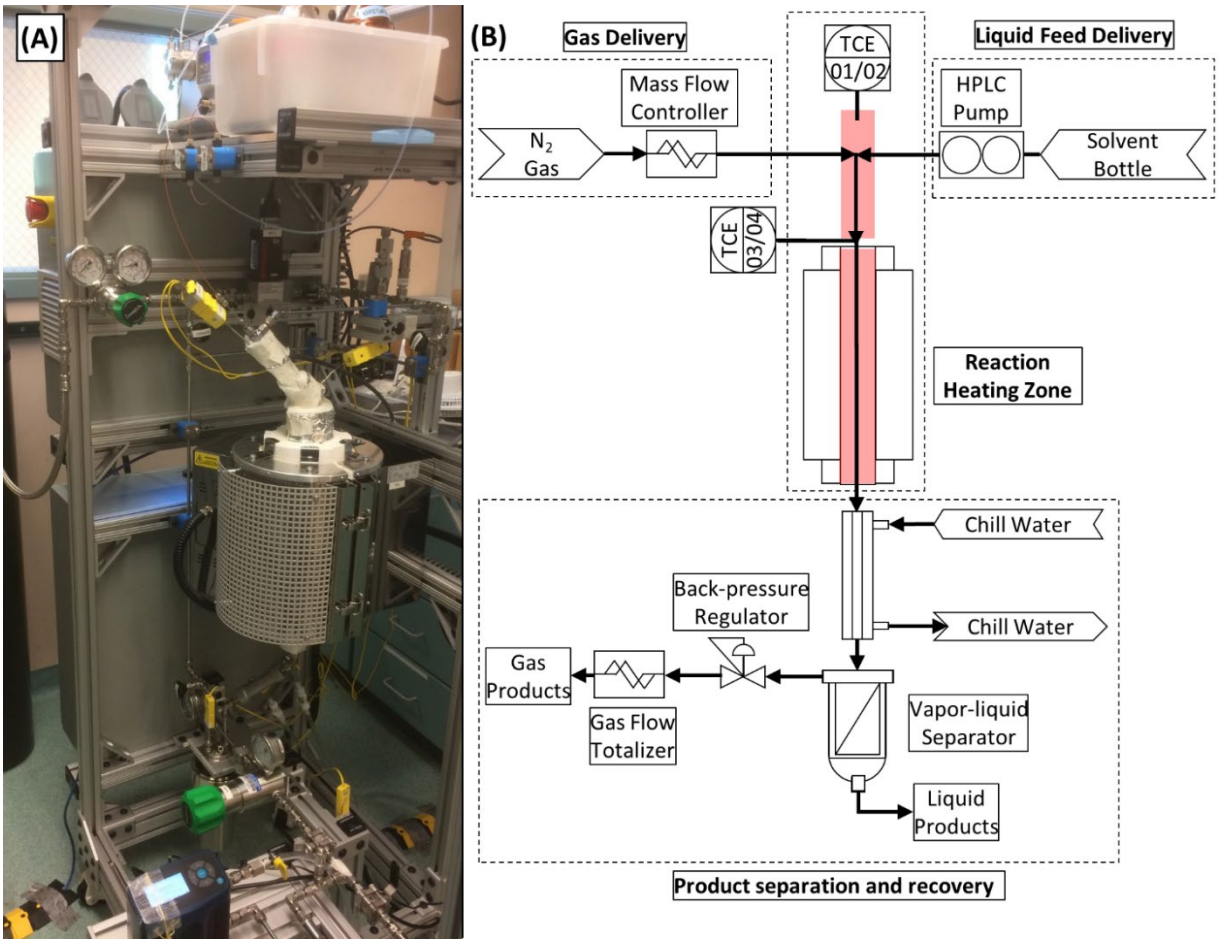

Figure S1. Fixed bed catalytic reactor used for performing experiments. (A) photograph and (B) general schematic.

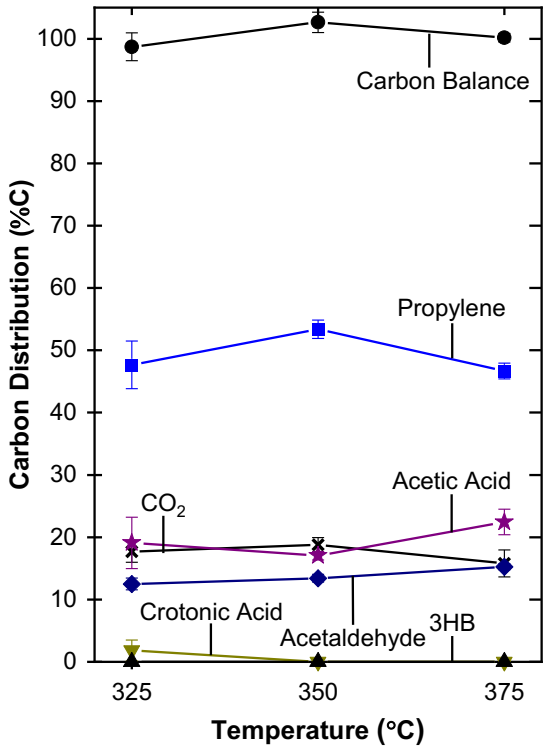

Figure S2. Effect of varying reactor bed temperature on carbon selectivity during vapor-phase conversion of 3HB over SIAL 3113 (as %C of inflow 3HB feed). Reaction conditions: WHSV of 3HB of 0.1 h^{-1}, 40 sccm N_2 at 55 psig (gaseous products sampled at atmospheric pressure), 4 h time-on-stream. Data points with error bars show the mean of duplicate reactions with min/max values.

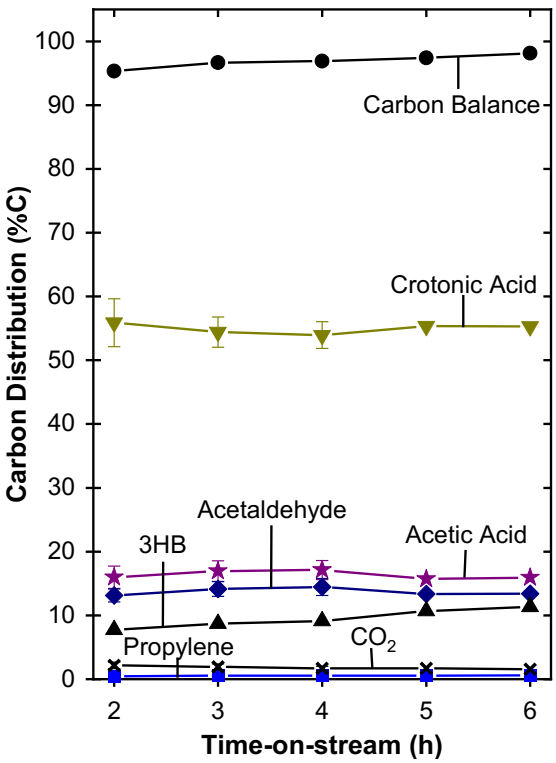

Figure S3. Carbon selectivity (as %C of inflow 3HB feed) results for 3HB "blank" reaction (no catalyst present) shown for the first 6 h time-on-stream. Reaction conditions: 350 °C, 0.3 mL/min of 2 wt% aqueous 3HB, 40 sccm N_2 at 55 psig (gaseous products sampled at atmospheric pressure). Data points with error bars show the mean of duplicate reactions with min/max values where duplicates were performed (up to 4 h).

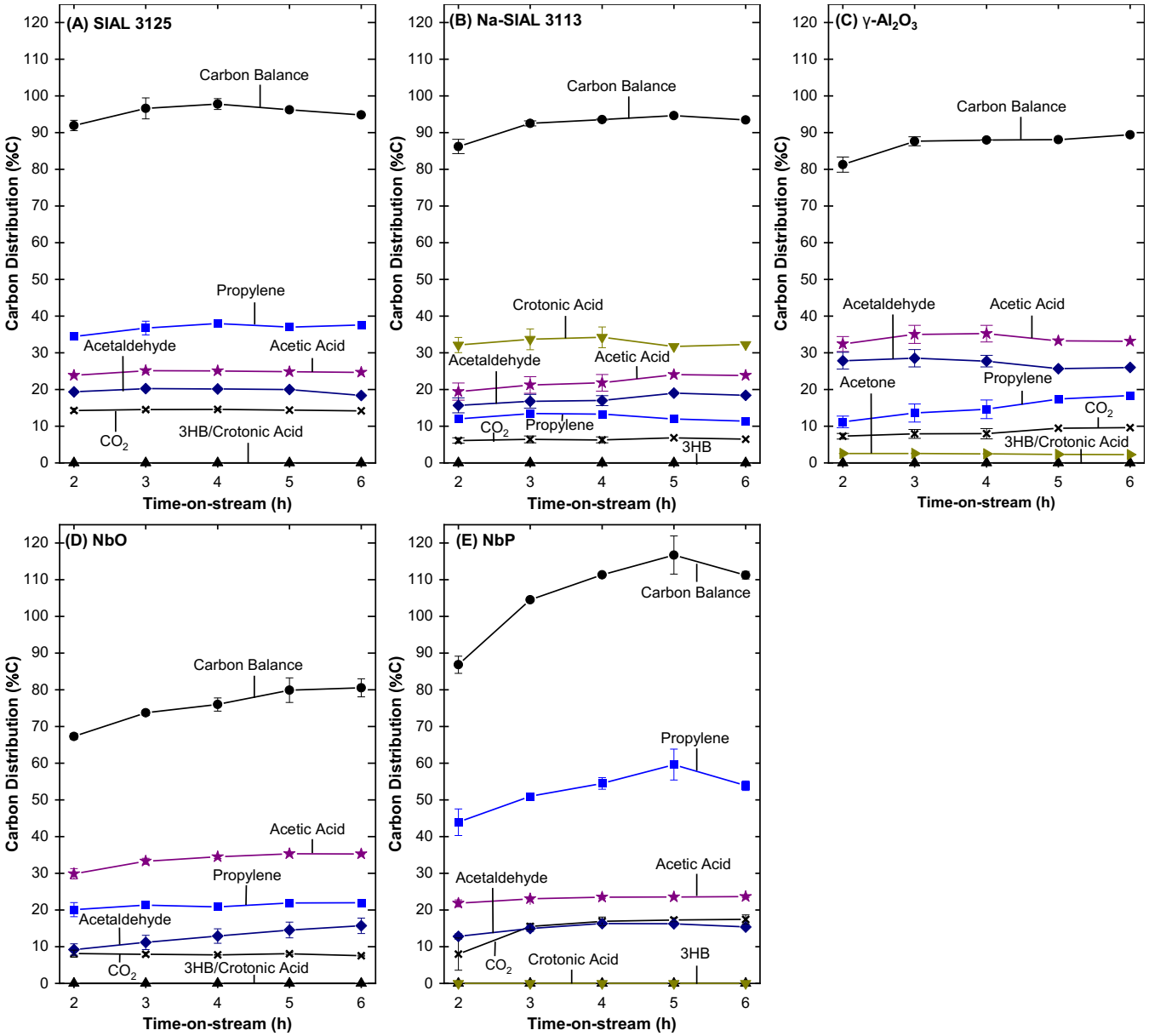

Figure S4. Detailed distribution of carbon products (as %C) during time-on-stream conversion of 3HB reaction over (A) SIAL 3125, (B) Na- SIAL 3113, (C) γ-Al_2O_3, (D) NbO, and (E) NbP corresponding to propylene yield data presented in **Figure 3a**. Reaction conditions: 350 °C, 0.1 h^{-1} WHSV, 40 sccm N_2 at 55 psig (gaseous products sampled at atmospheric pressure). Data points with error bars show the mean of duplicate reactions with min/max values where duplicates were performed.

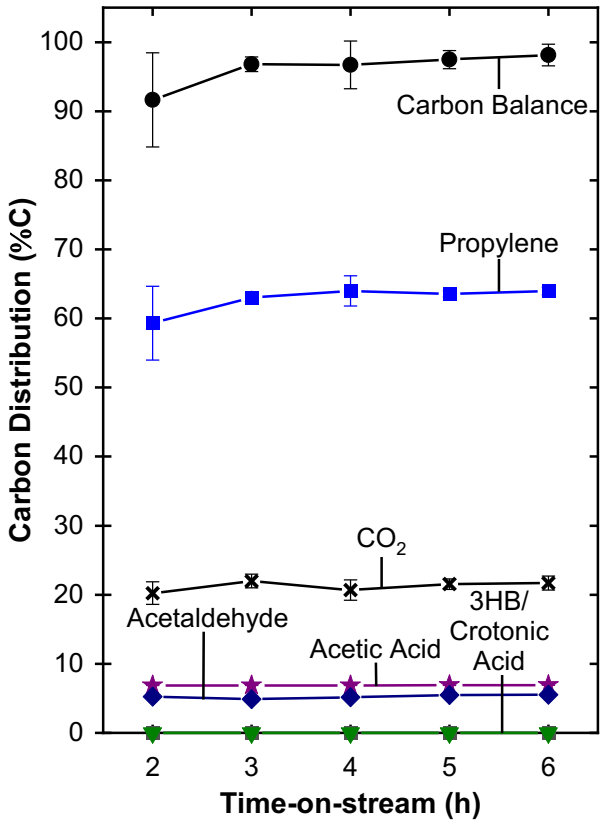

Figure S5. Distribution of carbon products (as %C of inflow crotonic acid feed) results for CA reaction over NbP. Reaction conditions: 350 °C, 0.1 h^{-1} WHSV, 40 sccm N_2 at 55 psig (gaseous products sampled at atmospheric pressure). Data points with error bars show the mean of duplicate reactions with min/max values. Horizontal dotted line indicates theoretical maximum yield of propylene from conversion of CA.

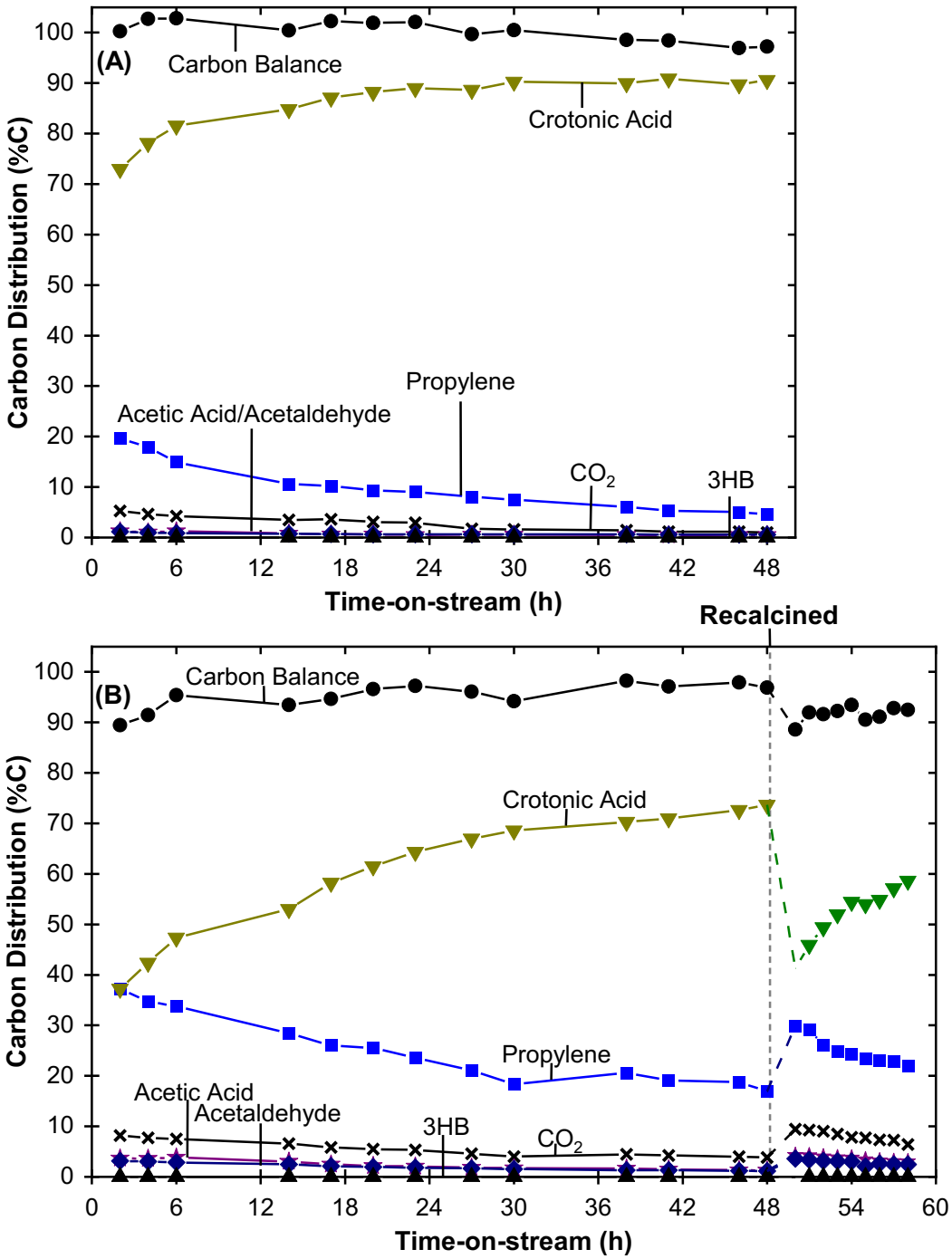

Figure S6. Detailed distribution of carbon products (as %C) during extended time-on-stream partial conversion of CA feeds for (A) SIAL 3113 and (B) NbP corresponding to the propylene yield data presented in **Figure 4.** Reaction conditions: 350 °C, 2.75 h^{-1} WHSV, 40 sccm N_2 at 55 psig (gaseous products sampled at atmospheric pressure). Recalcination conditions: 500 °C for 3 h (200 °C·h^{-1} heat rate).

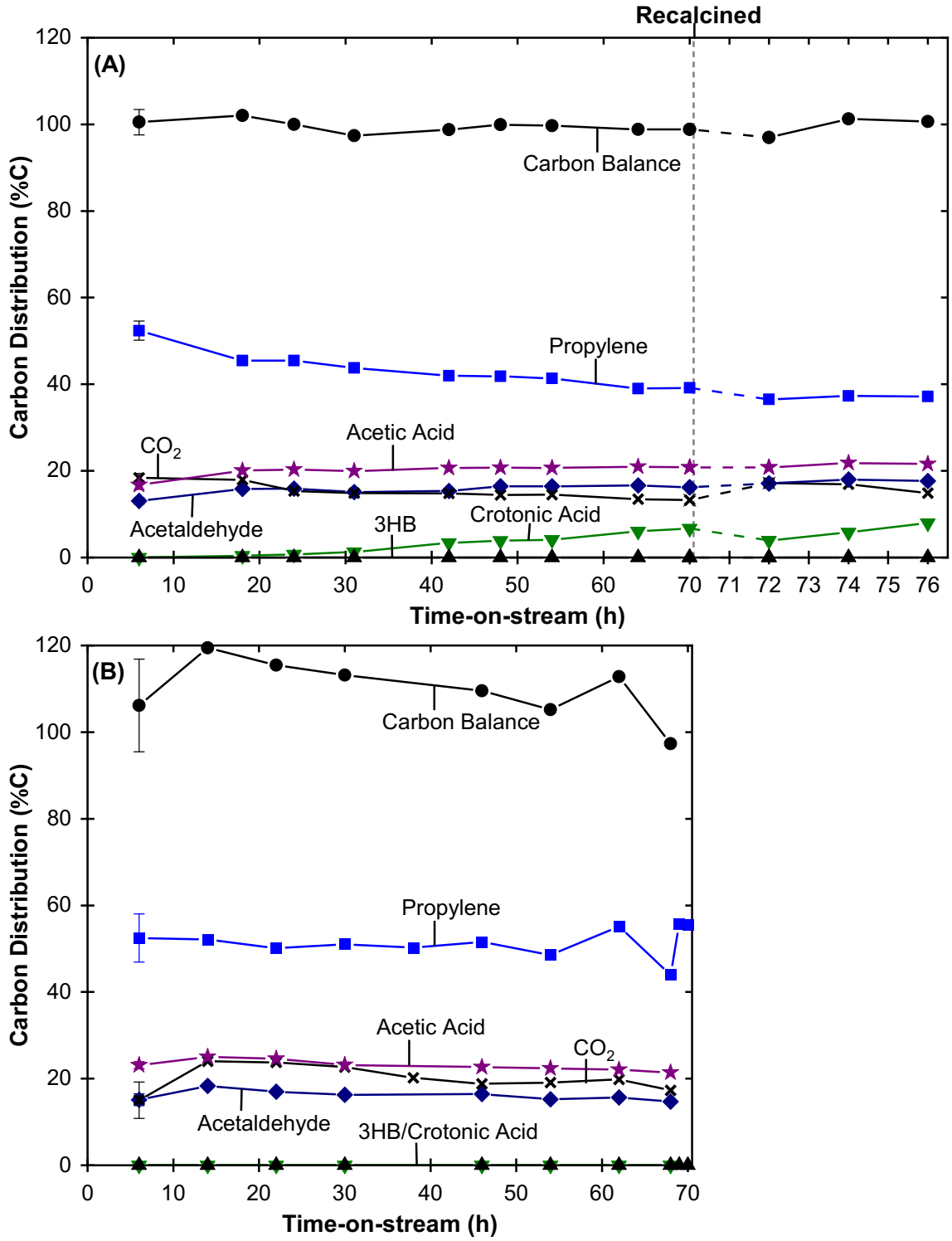

Figure S7. Detailed distribution of carbon products (as %C) during extended time-on-stream conversion of 3HB feeds for (A) SIAL 3113 and (B) NbP. SIAL 3113 subjected to recalcination at t = 70 h before continuing time-on-stream conversion measurements. Reaction conditions: 350 °C, 0.1 h^{-1} WHSV, 40 sccm N_2 at 55 psig (gaseous products sampled at atmospheric pressure). Recalcination conditions: 550 °C for 3 h (200 °C·h^{-1} heat rate).

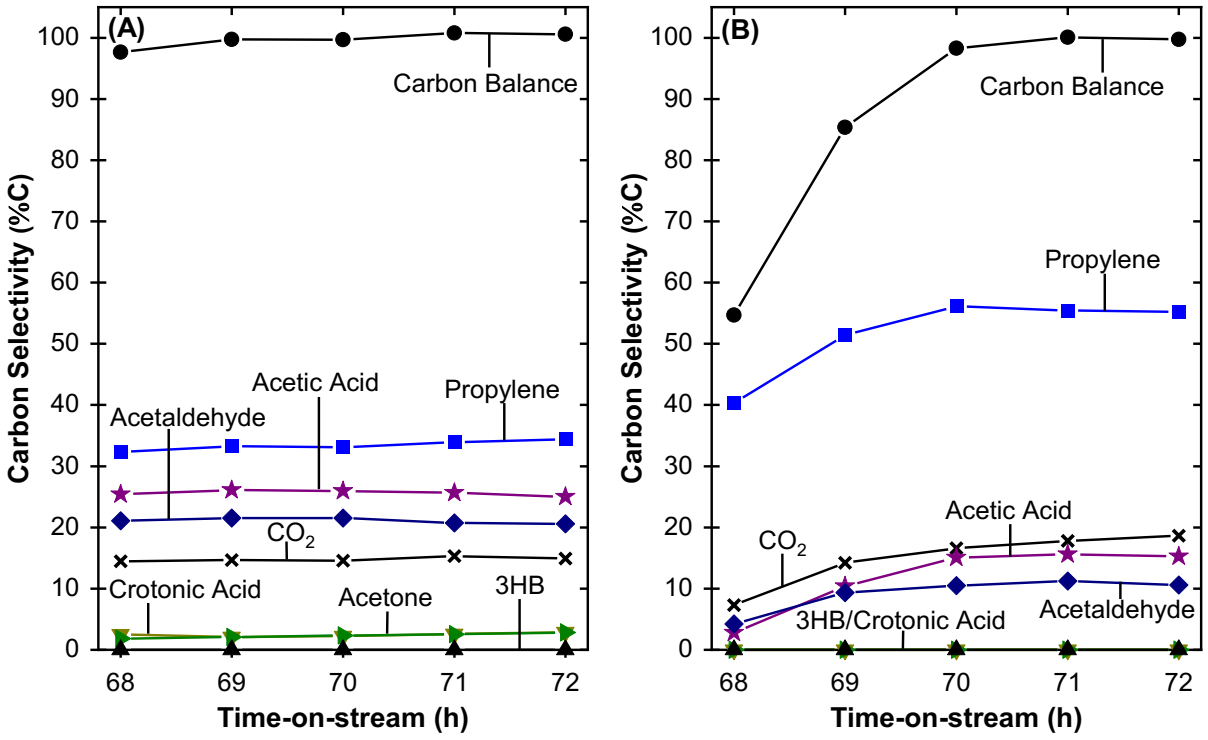

Figure S8. Carbon selectivity (as %C of inflow 3HB feed) of steam-treated SIAL 3113 (A) and NbP (B) for DYHD-DCBX of 3HB up to 6 h time-on-stream. Virgin catalysts were steam-treated for 66 h prior to starting 3HB feedstock (i.e., 68 h = 2 h time-on-stream of feedstock). Reaction conditions: 350 °C, 0.1 h^{-1} WHSV, 40 sccm N_2 at 55 psig (gaseous products sampled at atmospheric pressure).